PAPER • OPEN ACCESS

# Ion generation and loading of a Penning trap using pulsed laser ablation

New Journal of Physics
The open access journal at the forefront of physics

Deutsche Physikalische Gesellschaft DPG
IOP Institute of Physics

Published in partnership with: Deutsche Physikalische Gesellschaft and the Institute of Physics

OPEN ACCESS

RECEIVED
19 September 2019

REVISED
27 November 2019

ACCEPTED FOR PUBLICATION
10 December 2019

PUBLISHED
14 January 2020



PAPER

# Ion generation and loading of a Penning trap using pulsed laser ablation

**Muhammed Sameed**[1,2,3], **Daniel Maxwell**[2] and **Niels Madsen**[2]

[1] Department of Physics and Astronomy, University of Manchester, Manchester M13 9PL, United Kingdom
[2] Department of Physics, College of Science, Swansea University, Swansea SA2 8PP, Wales, United Kingdom
[3] Author to whom any correspondence should be addressed.

**E-mail:** m.sameed@cern.ch

**Keywords:** pulsed laser ablation, beryllium, sympathetic cooling, antihydrogen, ion generation, ion trapping, Penning trap

## Abstract

We investigated the production of aluminum and beryllium ions via pulsed laser ablation using 355 nm wavelength and 5 ns long laser pulses. The ablation threshold of $Al^+$ and $Be^+$ was measured to be $0.9 \pm 0.1$ (stat.) $\pm$ 0.3 (syst.) J cm$^{-2}$ and $1.4 \pm 0.1$ (stat.) $\pm$ 0.4 (syst.) J cm$^{-2}$ respectively. By employing electrostatic retarding potentials, the kinetic energy profile of the ablated ions was characterized as a function of laser fluence. Around the ablation threshold, we reliably produced between $10^8$ and $10^{10}$ ions, approximately 5% of which were dynamically trapped in a Penning–Malmberg trap.

## 1. Introduction

Trapped ions are routinely used for precision measurements [1–3] and quantum computing applications [4]. The need for ions is largely fulfilled by producing atoms from a resistively heated oven [5–9] and subsequently ionizing them using an electron or laser beam. To achieve the desired number of ions, an oven is typically operated for tens of seconds and at temperatures in excess of 500 K. Ions may also be loaded into a trap using a laser-cooled source of neutral atoms [10, 11], or directly via laser ablation of a target surface [12–17].

Presently, there is considerable interest in the antihydrogen trapping community to use beryllium ions to sympathetically cool positrons for antihydrogen production [18–21]. The antihydrogen trapping experiments take place in a Penning trap under extreme high vacuum ($P < 10^{-12}$ mbar) and cryogenic temperatures ($T < 100$ K). In such conditions, the use of a traditional atomic oven is unfeasible. Ovens produce a large and continuous flux of particles which is undesirable. The use of ovens also results in a significant heat load which is not suitable for experiments conducted in cryogenic environments. Laser ablation offers an alternative mechanism of ion creation that is more amenable to such vacuum and temperature constraints. Furthermore, geometrical constraints imposed by Penning traps requires the ablation target to be mounted axially far away from the trap electrodes, making direct production of ions that follow field-lines into the trap highly desirable.

Previous studies on the laser ablation of beryllium are sparse [22, 23]. Aluminum however has been the subject of several ablation studies using time-of-flight [24–26] and charge collection measurements [22, 27–29]. In all of these studies, significant ion production was typically observed for laser fluences around 1–2 J cm$^{-2}$. Such fluences are easily achievable using standard, commercially available pulsed laser sources. Moreover, ion formation with kinetic energies of several eV have been observed for laser fluences near the ablation threshold [26, 27, 29]. These energies are small enough that the ions can be dynamically trapped in a typical antihydrogen Penning trap. Studies with aluminum therefore allow us to benchmark our apparatus before moving onto beryllium.

In this paper we report on the production of aluminum and beryllium ions in vacuum by laser pulses incident on the respective metal ablation target. The particle yields were extracted by operating the target material as a Faraday Cup. Additionally, the kinetic energies of ejected charged particles were investigated using electrostatic blocking potentials. The kinetic energy distributions (KEDs) of the emitted $Al^+$ and $Be^+$ ions were

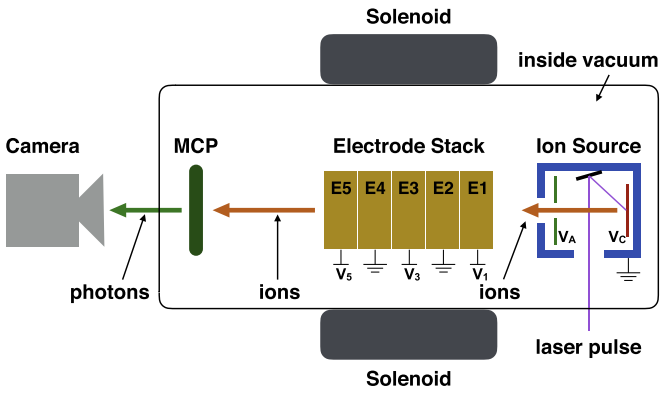


**Figure 1.** Simplified schematic of the experimental setup. A laser pulse is focused on a metal target generating ions. The solenoid magnetic field guides the ions from the source to the MCP. The electrode stack can be used to block, trap, and/or accelerate the ions. The ions can be ejected to the combined MCP-Phosphor detector, which generates light. A camera situated just outside the vacuum region of the ablation chamber images the light. The components are not drawn to scale.

analyzed for several different laser fluences (up to 2 J cm$^{-2}$ and 4 J cm$^{-2}$ for aluminum and beryllium respectively). We also report a set of successful attempts to hold $Be^+$ ions in a Penning–Malmberg trap for several seconds. We confirm the viability of pulsed laser ablation as a potential mechanism to deliver enough trappable $Be^+$ ions to sympathetically cool positrons in ALPHA [20].

## 2. Experiment

The experimental setup is comprised of a vacuum chamber (background pressure $<5 \times 10^{-8}$ mbar), a metal ablation target (aluminum or beryllium), a Penning–Malmberg trap, a combined dual micro-channel plate and phosphor screen detector (Photonis, model: QS19930A-1), and an electronic system for data acquisition and analysis. A schematic for the setup is shown in figure 1, and a scaled drawing of the apparatus is provided in figure 2(a).

To produce the laser-ablated plasma, we used frequency-tripled Nd:YAG laser pulses at 355 nm wavelength and 5 ns pulse length (FWHM). The laser pulses hit the metal target (purity >99%, thickness ~0.5 mm) at an incidence angle of approximately 50° with respect to the target normal. The laser beam was focused by a 25 cm focal length lens onto the target surface. The laser beam waist ($1/e^2$ radius) was measured to be 16.6 $\pm$ 2.5 $\mu$m by passing a knife edge across the beam and inferred by analysis of burn patterns on exposed burn paper. The laser energy was monitored by a calibrated photodiode showing a shot-to-shot fluctuation within 10% of the average value. The overall uncertainty on the value of the laser fluence is mainly due to the systematic uncertainty in the determination of the spot size.

A single measurement consists of a laser pulse that is reflected by a mirror and hits the ablation target (see figures 1 and 2(c)). Ions generated are accelerated by the acceleration plate, with some of the ions passing through the aperture as a divergent beam. The target (cathode) and acceleration plate (anode) are electrically insulated from each other, and an external power supply can be used to apply a potential bias on each of these components ($V_C$ and $V_A$ for cathode and anode respectively). The five electrodes of the stack along with an external solenoid form a Penning–Malmberg trap. The magnetic field from solenoid serves to guide the ions from the source to the MCP, and to confine the ions radially for trapping. As shows in figure 2(b), the peak field at the center of the trapping region is about 900 Gauss. Ions reaching the electrodes may therefore be blocked, trapped, accelerated/decelerated, or simply allowed to pass through. Ions exiting the electrode stack are detected at the MCP detector and imaged by a CCD camera.

The target was biased at $V_C = +40$V in order to accelerate the ions away from the surface. A $V_A = -10$V accelerating potential assisted in removing the ablated ions from the target and reducing the divergence of the beam. The release of laser-ablated ions resulted in a momentary (~2 $\mu$s) charge deficit on the target surface, which was recorded by a digitizing oscilloscope (Tektronix, model: DPO5104).

Beyond the electrode stack, the ions were detected at the MCP detector whose front, back, and phosphor screen were biased at −600 V, 800 V, and 4400 V respectively. By means of a pickoff circuit connected to the front of the MCP, the charge arriving at the MCP front was recorded. The MCP and camera were used to concurrently image the radial distribution of the charges. In this manner, it was possible to calibrate the intensity of the acquired image against the total charge arriving at the MCP front.

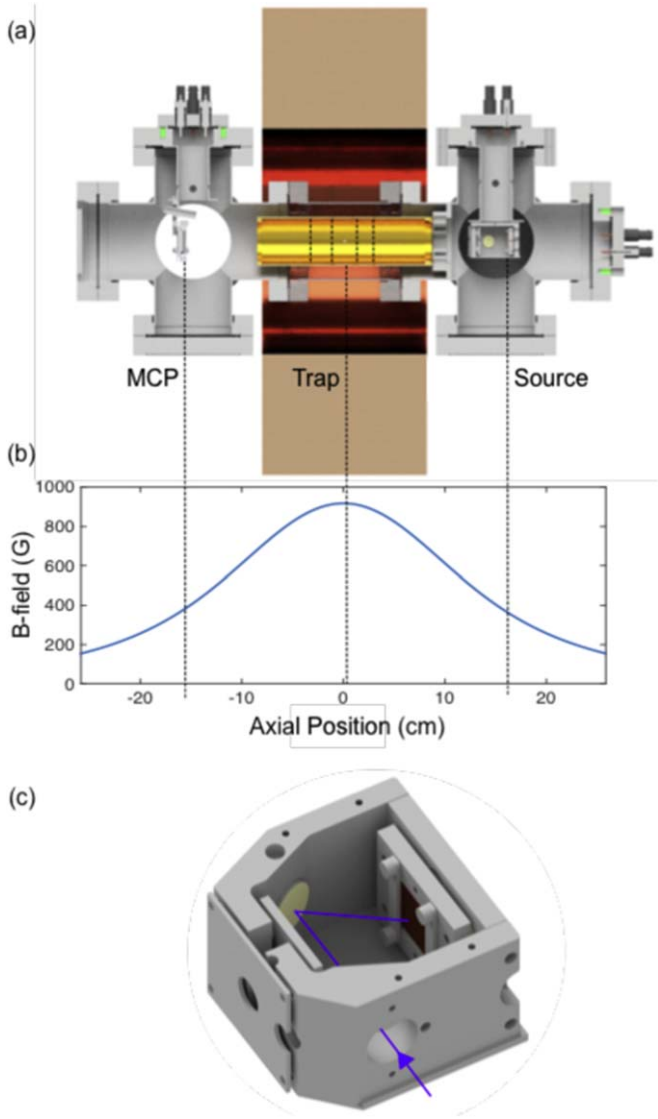


**Figure 2.** (a) Scaled half-section view of the key components of the apparatus. (b) On-axis magnetic field strength plotted as a function of axial position. (c) Scaled drawing of the ion source. The purple arrow shows the path taken by the laser pulse to reach the ablation target.

## 3. Results and discussion

### 3.1. Singly charged ion ablation threshold and total charge yield

By lowering the pulse energy sufficiently, the laser fluence can be lowered to the point where the ablation signal is below the background level. This gives us a measurement of the upper limit on the minimum fluence required for ion production, also known as the ablation threshold. In our setup, a minimum charge, $|Q/e| > 10^8$ (where $Q$ is the total charge and $e$ is the charge of the electron), must be ablated to produce a signal that is distinguishable from background.

The total charge that leaves the aluminum and beryllium targets as a result of laser ablation is shown in figure 3. For the lowest pulse energy of 10 $\mu$J used in this experiment (fluence 0.9 J cm$^{-2}$), the ablation signal is just above background for $Al^+$, with a yield of ~0.2 $\times$ $10^9$ charges. This implies that the ablation threshold for aluminum lies below 0.9 J cm$^{-2}$, consistent with a previously reported value of 0.8 J cm$^{-2}$ for analogous laser parameters [26] . Similarly in the case of beryllium, the ablation threshold for singly-charged ions lies just below 1.4 J cm$^{-2}$, nearly 50% larger than the estimate for $Al^+$. Given that the melting point of beryllium (1560 K) is a factor of ~1.67 larger than that of aluminum, the higher ablation threshold for beryllium is qualitatively consistent with earlier reports where metals with high melting points are observed to have relatively higher ablation thresholds for singly-charged ions [29].

For fluences above 1.1 J cm$^{-2}$ in aluminum and 2.9 J cm$^{-2}$ in beryllium, the charge yield increases linearly. Similar ion yield increases with fluence have previously been reported [25].

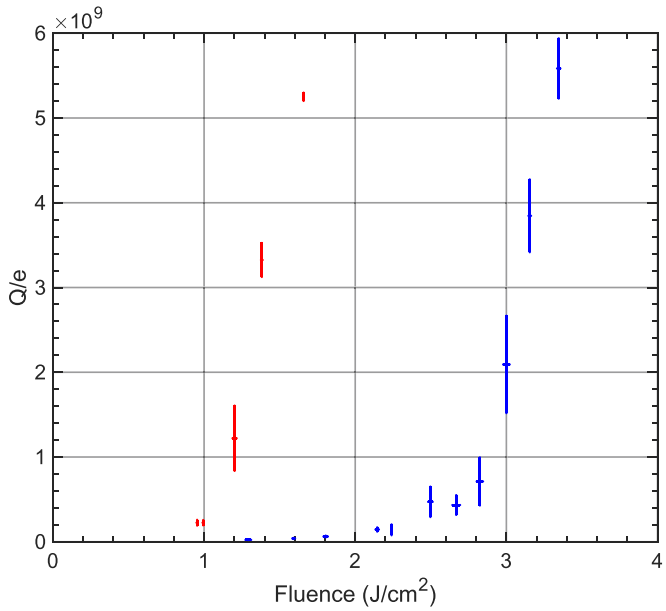


**Figure 3.** Number of charges leaving the aluminum (red) and beryllium (blue) ablation targets as a function of laser fluence. The error bars at each data point are standard errors of the mean. We observe an ablation threshold of 0.9 J cm$^{-2}$ for aluminum and 1.4 J cm$^{-2}$ for beryllium.

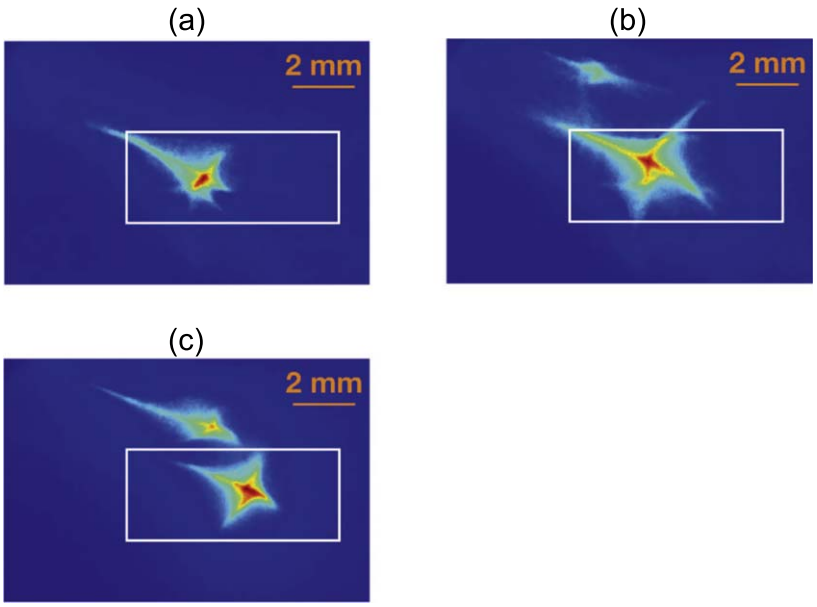


**Figure 4.** Typical MCP images from ablating the aluminum target with (a) 1.4, (b) 1.9, and (c) 2.3 J cm$^{-2}$ laser pulses. The white rectangle defines the region of interest that separates the primary cloud from the rest of the image. All pictures use the same length scale but different intensity scaling.

### 3.2. Ion KED

To measure the KED of the ablated species, blocking potentials between 0 and 150 V were applied on electrode E3. The emitted particles from the source that successfully crossed the potential barrier and passed through the Penning trap were incident on the MCP and the resulting light was imaged by the CCD camera.

Figure 4 shows typical MCP images for the ablation of aluminum at three different fluences. At a fluence of 1.4 J cm$^{-2}$, only one cloud of charges was seen. At the 1.9 and 2.3 J cm$^{-2}$ however, two distinct clouds of charges were observed. The appearance of the secondary cloud at higher fluences may indicate the production of doubly-charged aluminum ions, suggesting an ablation threshold for $Al^{2+}$ between 1.4 and 1.9 J cm$^{-2}$. Within the measurement error, this is consistent with previously reported thresholds of 3 J cm$^{-2}$ [25] and 1.4 J cm$^{-2}$ [26].

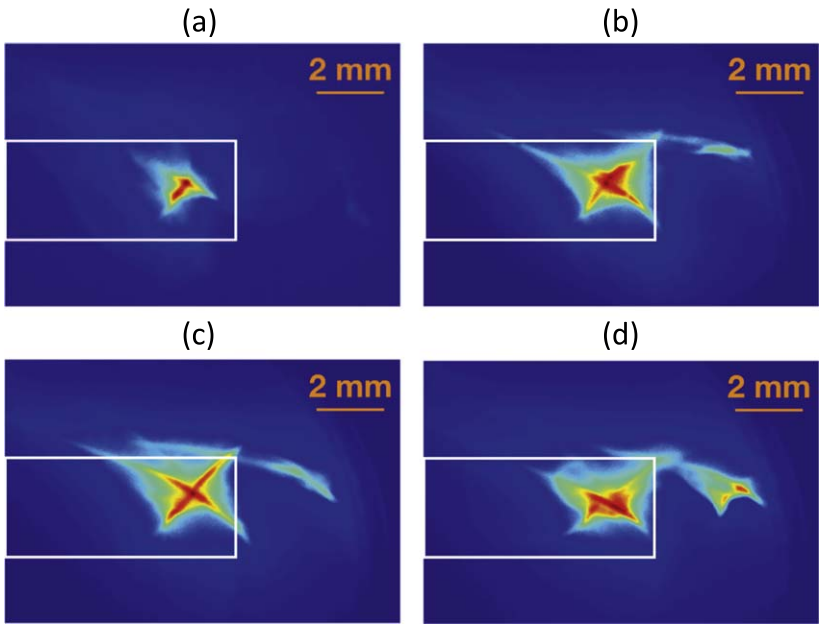


**Figure 5.** Typical MCP images from ablating the beryllium target with (a) 2.3, (b) 2.7, (c) 3.1, and (d) 3.5 J cm$^{-2}$ laser pulses. The white rectangle defines the region of interest that separates the primary cloud from the rest of the image. All pictures use the same length scale but different intensity scaling.

Figure 5 shows typical MCP images for the ablation of beryllium at four different fluences. At a fluence of 2.3 J cm$^{-2}$, only one cloud of charges was seen. At the 2.7, 3.1 and 3.5 J cm$^{-2}$, two distinct clouds of charges were observed, indicating as before the production of doubly-charged ions. This suggests a fluence threshold between 2.3 and 2.7 J cm$^{-2}$ for $Be^{2+}$. The fluence threshold of $Be^{2+}$ has not previously been reported.

In figures 4 and 5, we observe that ions hitting the MCP result in a star-shaped image. Additionally, singly and doubly charged ion species appear to separate. Both of these features occur due to stray electric fields near the front of the MCP. We identified these effects at a later date with a similar, independent experimental setup. At the time of data taking, we had not anticipated these effects and did not have the ability to remove these stray fields.

We define a region of interest (shown by a white rectangle in figures 4 and 5) that includes the primary cloud but avoids the secondary cloud in all of the recorded MCP images. A measure of the number of singly-charged ions can then be obtained by summing the intensities of all of the pixels within this region and subtracting the background, which we call the MCP image intensity. In order to extract a KED of singly-charged ions from these MCP images, we take the average MCP image intensity at each blocking potential and perform a least-squares fit to a cumulative double Maxwell–Boltzmann distribution function.

Figure 6 shows the aluminum KED data and resulting double Maxwell–Boltzmann fits at three different fluences. The consistency of the fits to the data may be interpreted as the charges originating due to two separate ion formation processes. Similar observations have previously been reported in [26].

The beryllium KED data and associated double Maxwell–Boltzmann fits at five different fluences are shown in figure 7. As with aluminum, the fits to the data are consistent with the charges originating from two separate ion formation processes. Due to the large error bars on some of our data points, we emphasize only the qualitative nature of our results and note that higher fluences generally result in the production of more energetic ions.

### 3.3. $Be^{+}$ trapping

The following sequence was used to dynamically trap ions from the ion source and subsequently image them on the MCP:

1. Erect a potential barrier for the ions by applying an electric potential on E5.
2. Transmit a single laser pulse to the ablation target to create ions.
3. Wait a specified amount time to allow ions from the ion source to enter the electrode stack.
4. Apply an electrode potential on E1 to trap the ions inside the stack.

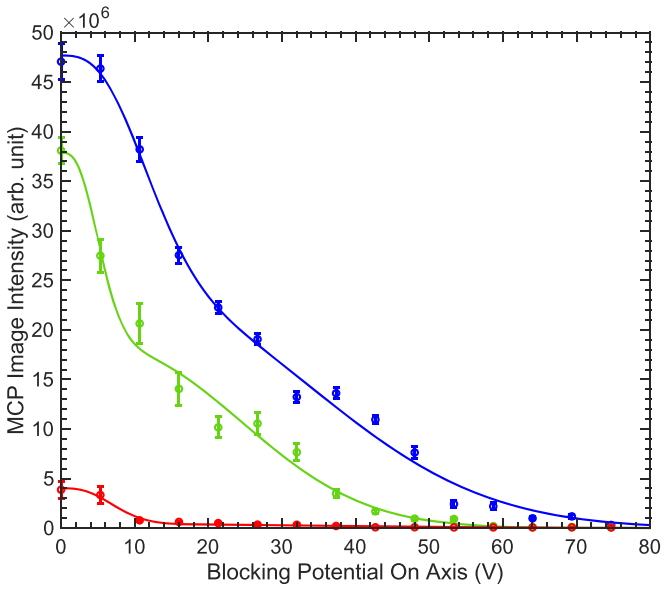


**Figure 6.** MCP image intensity as a function of the on-axis blocking potential from ablating the aluminum target with 1.4 (red), 1.9 (green), and 2.3 (blue) J cm$^{-2}$ laser pulses. The error bars shown are standard errors of the mean. A double Maxwell–Boltzmann cumulative distribution function is fitted to each dataset.

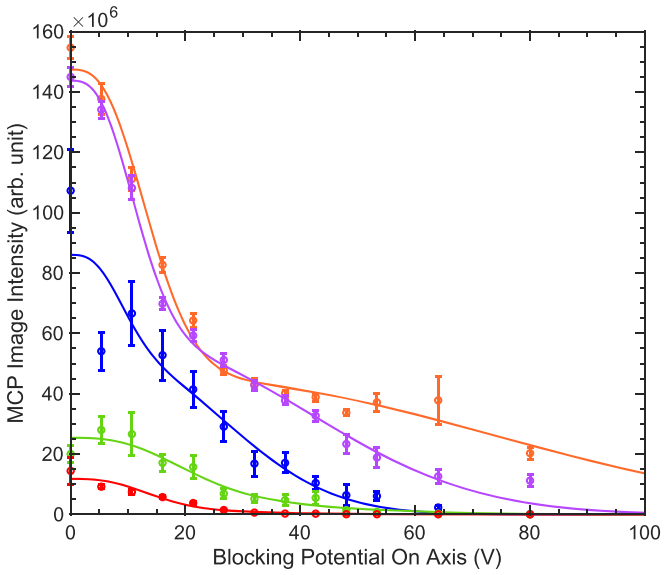


**Figure 7.** MCP image intensity as a function of the on-axis blocking potential from ablating the beryllium target with 1.9 (red), 2.3 (green), 2.7 (blue), 3.1 (purple), and 3.5 (orange) J cm$^{-2}$ laser pulses. The error bars shown are standard errors of the mean. A double Maxwell–Boltzmann cumulative distribution function is fitted to each dataset.

5. Hold the trapped ions for the desired duration.

6. Dump the trapped ions onto the MCP by quickly (∼1 $\mu$s) dropping the potential on E5 to 0 V.

Beryllium ions were successfully trapped at a laser pulse energy of 300 $\mu$J and fluence of 2.9 J cm$^{-2}$. 200 V potentials were applied to both E1 and E5, and a gate delay of 8 $\mu$s was used. The intensity of the observed MCP image corresponded to approximately 1.7 $\times$ 10$^8$ trapped ions.

Figure 8 shows the number of trapped $Be^+$ ions as a function of holding time. The ions were held for a minimum of 3 s, up to 22 s. The average number of trapped ions was 1.6 $\times$ 10$^8$ ions, more than two orders of magnitude higher than what is required for the sympathetic cooling of positrons in the ALPHA antihydrogen experiment [20].

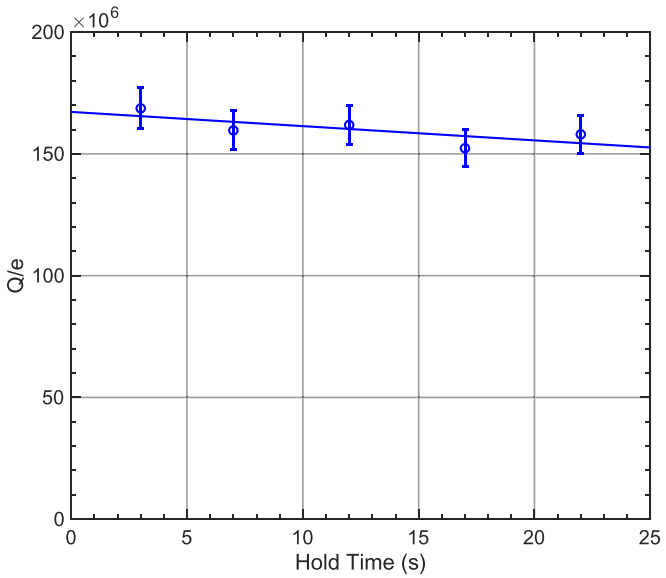


**Figure 8.** Number of trapped $Be^+$ ions as a function of hold time. The average number of trapped ions was $1.6 \times 10^8$. The total number of trapped ions decreased linearly for increasing hold times.

In order to estimate the trapping efficiency, we note that when the the trapping electrodes are grounded, the ions striking the MCP saturate the MCP image, with the image intensity corresponding to the arrival of at least $3 \times 10^9$ ions. Using this value, we determine an upper bound for the trapping efficiency at 5.3%.

## 4. Conclusion

We have investigated the production of aluminum and beryllium ions using single 355 nm ablation pulses. The production of $Al^+$ requires at least 0.9 J $cm^{-2}$ laser fluence whereas the ablation threshold for $Al^{2+}$ is between 1.4 and 1.9 J $cm^{-2}$. In our experiments, we observe higher ion yields and higher kinetic energies with increasing laser fluence. For fluences up to 2.3 J $cm^{-2}$, most of the aluminum ions produced have axial kinetic energies less than 80 eV. The observed fluence thresholds and KEDs are consistent with available literature on aluminum ablation, making our test apparatus a reliable tool to study other metals of interest, in particular beryllium.

For beryllium, at least 1.4 J $cm^{-2}$ laser fluence is required to produce $Be^+$ and between 2.3 and 2.7 J $cm^{-2}$ for $Be^{2+}$. As with aluminum, using higher fluences for ablation result in more energetic ions and larger ion yields. Fluences up to 3.0 J $cm^{-2}$ may be employed to produce ions that have kinetic energies less than 80 eV and ion yields in excess of $10^9$, suitable for trapping in ALPHA.

By choosing appropriate electrode potentials and gate timing, ions released by the source were trapped in a Penning–Malmberg trap. For the trap used in our experiment, the electrode stack is relatively short compared to the nominal bunch length of the ion cloud, therefore only a small fraction of ions may be trapped. The trap in ALPHA is significantly longer however, so we expect a much higher trapping efficiency.

## Acknowledgments

This work was supported by EPSRC. We thank the ALPHA Collaboration for lending us the trap electrodes and the solenoid magnet. We thank Jack Segal for his assistance in the aluminum ablation measurements. We thank Dr. William Bertsche for discussions and feedback.

## ORCID iDs

Muhammed Sameed https://orcid.org/0000-0002-9706-8970
Daniel Maxwell https://orcid.org/0000-0001-5178-9492
Niels Madsen https://orcid.org/0000-0002-7372-0784

## References


[1] Thompson R 1990 Precision measurement aspects of ion traps *Meas. Sci. Technol.* **1** 93
[2] Ivanov P A, Vitanov N V and Singer K 2016 High-precision force sensing using a single trapped ion *Sci. Rep.* **6** 28078
[3] Cairncross W B *et al* 2017 Precision measurement of the electron's electric dipole moment using trapped molecular ions *Phys. Rev. Lett.* **119** 153001
[4] Bruzewicz C D, Chiaverini J, McConnell R and Sage J M 2019 Trapped-ion quantum computing: progress and challenges *Appl. Phys. Rev.* **6** 021314
[5] Lucas D *et al* 2004 Isotope-selective photoionization for calcium ion trapping *Phys. Rev.* A **69** 012711
[6] Nagy S *et al* 2006 New mass value for $^{7}$Li *Phys. Rev. Lett.* **96** 163004
[7] Crick D, Ohadi H, Bhatti I, Thompson R and Segal D 2008 Two-ion Coulomb crystals of $Ca^{+}$ in a Penning trap *Opt. Express* **16** 2351
[8] Thompson R, Donnellan S, Crick D and Segal D 2009 Applications of laser cooled ions in a penning trap *J. Phys. B: At. Mol. Opt. Phys.* **42** 154003
[9] Andelkovic Z *et al* 2013 Laser cooling of externally produced Mg ions in a Penning trap for sympathetic cooling of highly charged ions *Phys. Rev.* A **87** 033423
[10] Sage J M, Kerman A J and Chiaverini J 2012 Loading of a surface-electrode ion trap from a remote, precooled source *Phys. Rev.* A **86** 013417
[11] Bruzewicz C D, McConnell R, Chiaverini J and Sage J M 2016 Scalable loading of a two-dimensional trapped-ion array *Nat. Commun.* **7** 13005
[12] Davies D *et al* 2007 A high-power laser ablation ion source for Penning trap studies of nuclear reaction products *J. Phys.: Conf. Ser.* **59** 136
[13] Leibrandt D R *et al* 2007 Laser ablation loading of a surface-electrode ion trap *Phys. Rev.* A **76** 055403
[14] Sheridan K, Lange W and Keller M 2011 All-optical ion generation for ion trap loading *Appl. Phys.* B **104** 755
[15] Zimmermann K, Okhapkin M, Herrera-Sancho O and Peik E 2012 Laser ablation loading of a radiofrequency ion trap *Appl. Phys.* B **107** 883
[16] Borisyuk P V *et al* 2017 Loading of mass spectrometry ion trap with Th ions by laser ablation for nuclear frequency standard application *Eur. J. Mass Spectrom.* **23** 146
[17] Niemann M, Meiners T, Mielke J, Borchert M J, Cornejo J M, Ulmer S and Ospelkaus C 2020 Cryogenic $^{9}Be^{+}$ Penning trap for precision measurements with (anti-)protons *Meas. Sci. Technol.* **31** 035003
[18] Jelenković B, Newbury A, Bollinger J, Mitchell T and Itano W M 2002 Sympathetically laser-cooled positrons *Nucl. Instrum. Methods Phys. Res.* B **192** 117
[19] Jelenković B, Newbury A, Bollinger J J, Itano W M and Mitchell T 2003 Sympathetically cooled and compressed positron plasma *Phys. Rev.* A **67** 063406
[20] Madsen N, Robicheaux F and Jonsell S 2014 Antihydrogen trapping assisted by sympathetically cooled positrons *New J. Phys.* **16** 063046
[21] Ahmadi M *et al* 2017 Antihydrogen accumulation for fundamental symmetry tests *Nat. Commun.* **8** 681
[22] Knight R 1981 Storage of ions from laser-produced plasmas *Appl. Phys. Lett.* **38** 221
[23] Thompson C A and Andrews L 1994 Reactions of laser ablated Be atoms with $O_2$: infrared spectra of beryllium oxides in solid argon *J. Chem. Phys.* **100** 8689
[24] Alimpiev S, Belov M and Nikiforov S 1993 Laser ablation/ionization technique for trace element analysis *Anal. Chem.* **65** 3194
[25] Amoruso S *et al* 1996 Laser produced plasmas in high fluence ablation of metallic surfaces probed by time-of-flight mass spectrometry *Appl. Surf. Sci.* **96** 175
[26] Apinániz J I *et al* 2008 Ion kinetic energy distributions and mechanisms of pulsed laser ablation on Al *J. Phys. Chem.* C **112** 16556
[27] Ooie T, Yano T, Yoneda M and Katsumura M 2000 An ion source using laser ablation *J. Laser Appl.* **12** 171
[28] Torrisi L, Borrielli A and Margarone D 2007 Study on the ablation threshold induced by pulsed lasers at different wavelengths *Nucl. Instrum. Methods Phys. Res.* B **255** 373
[29] Baraldi G, Perea A and Afonso C N 2011 Dynamics of ions produced by laser ablation of several metals at 193 nm *J. Appl. Phys.* **109** 043302